Supporting Information

# Microwave-Assisted Evolution of $WO_3$ and $WS_2/WO_3$ Hierarchical Nanotrees

Noho Lee[a†], Junghyeok Kwak[a†], Ji Hye Kwak[b], Sang-Mun Jung[a], Jaerim Kim[a], Anupam Giri[a], Kaliannan Thiyagarajan[a], Yong-Tae Kim[a], Sunshin Jung[b*], Jong Kyu Kim[a*] and Unyong Jeong[a*]

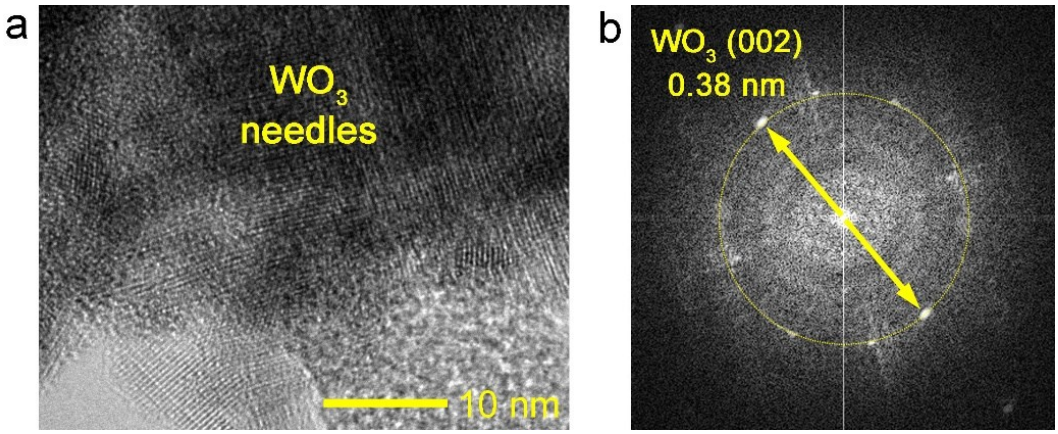


**Figure S1.** (a) TEM image taken from overlapped $WO_3$ nanoneedles. Lattice spacing with various directions are visible. (b) Fast Fourier transform (FFT) image obtained from (a). Bright spots are visible on yellow circle which corresponds to $WO_3$ (002) d-spacing.

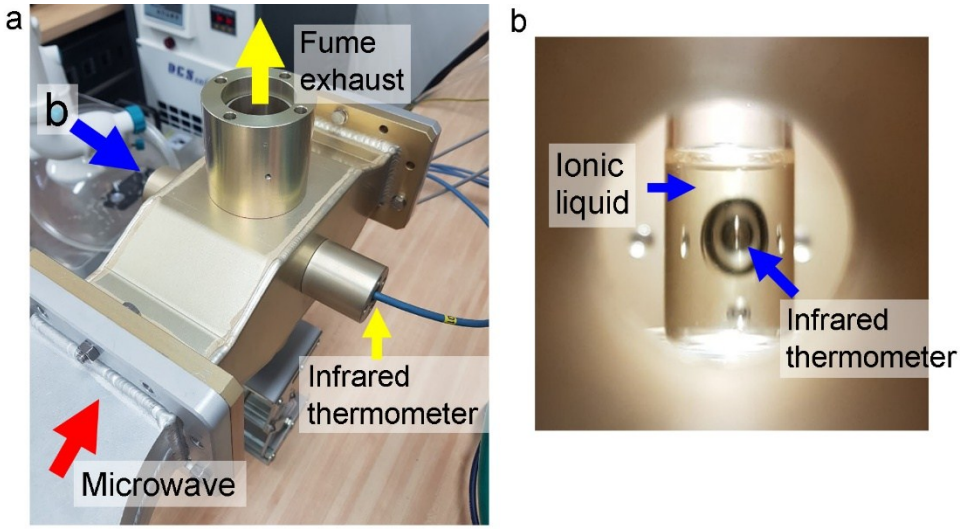


**Figure S2.** Camera images of microwave heating setup used for temperature and absorption measurement.

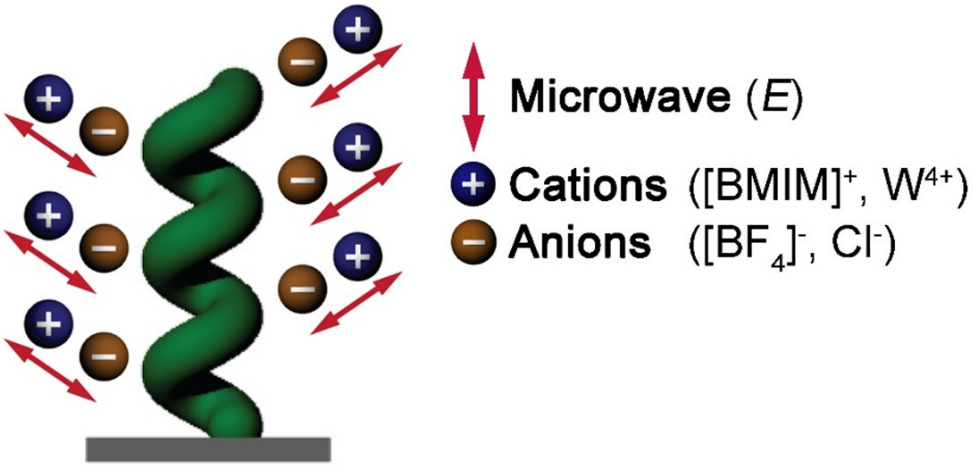


**Figure S3.** Schematic description of aligned cations and anions along with microwave irradiation

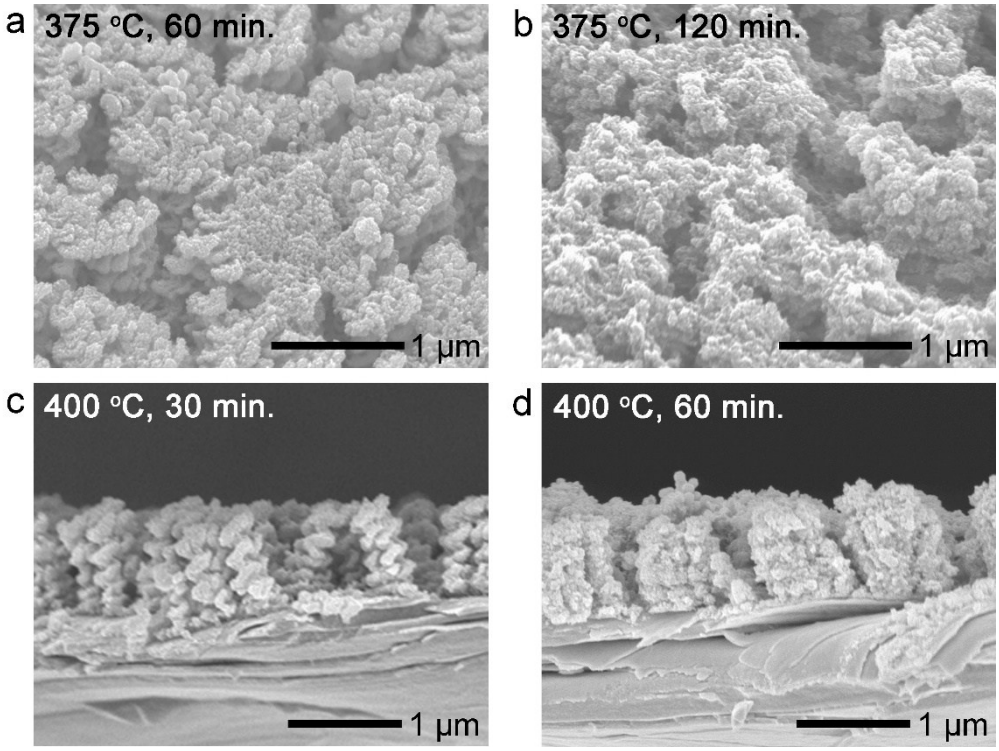


**Figure S4.** SEM images of $WO_3$ helix-needle samples prepared by non-microwave conventional heating with (a) 375 °C, 60 min., (b) 375 °C, 120 min., (c) 400 °C, 30 min., (d) 400 °C, 60 min.

## Cyclic Voltammonograms at various scan rate

To compare the surface area, cyclic voltammograms of the $WO_3$ nanotree and the $WO_3$ nanohelix were collected at various scan rate with region of 0.15 ~ 0.25 $V_{RHE}$. W foil was also used as control sample. As the scan rate increases, the $WO_3$ nanotree sample shows a significantly larger increase in current density than the other samples (Fig. S5c). The current density change at a different scan rate is mainly due to the scan rate dependence of capacitive current. In addition, capacitive current depends on the surface area of electrode. Thus, the larger increase in current density with increasing scan rate for the $WO_3$ nanotree compared the $WO_3$ nanohelix and the W foil can be attributed to the larger surface area of the nanotree structure. Although small faradaic current caused by the formation of $H_xWO_3$ in the measured region (0.15 ~ 0.25 $V_{RHE}$) can contributed to the increase in current as the scan rate increases, the increase in capacitive current is expected to be dominante.[1]

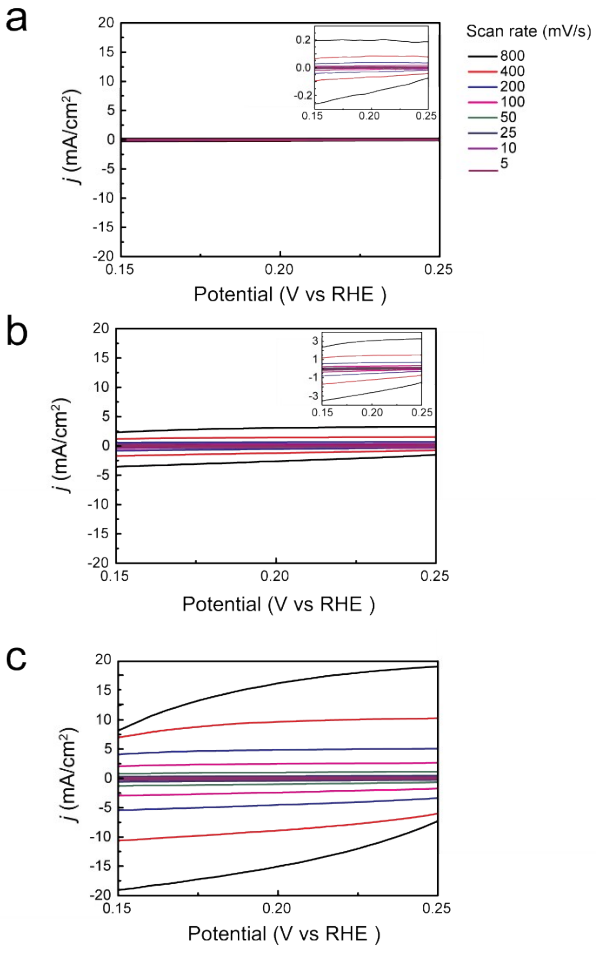


**Figure S5.** Cyclic voltammograms of (a) W foil, (b) $WO_3$ nanohelix and (c) $WO_3$ nanotree collected at various scan rate with region of 0.15 ~ 0.25 $V_{RHE}$. The insets show magnified images.

## Electrochromic reaction of $WO_3$ in cathodic condition

As shown in Fig. S6a, when the −0.3 $V_{RHE}$ was applied to the $WO_3$ nanohelix using a chronoamperometry, the color changes from light grey to deep blue in a few seconds (Fig. S6a and S6b). The color change of the $WO_3$ sample is attributed to the injection of electrons and ions in the $WO_3$, which can be expressed as follows[2,3]:

$$WO_3 + xH^+ + xe^- \rightarrow H_xWO_3$$

In addition, electrochromism of the $WO_3$ in the $WS_2/WO_3$ nanotrees was investigated by using XPS. For the electrochromic reaction, −0.3 $V_{RHE}$ was applied to the $WS_2/WO_3$ nanotree sample for 60s using the chronoamperometry in 0.5 M $H_2SO_4$. Fig. S7 shows the XPS spectrum of O1s for $WS_2/WO_3$ nanotree sample before and after the electrochromic reaction.

As shown in Fig. S7a, the spectrum shows the major peak at the binding energy of 530.16 eV, assigned to the $O^{2-}$ of $WO_3$. After the electrochromic reaction, the peak shows broadening and shift to higher binding energy, which can be deconvoluted into two components. As shown in Fig. S7b, the higher energy peak at 531.63 eV can be assigned to the hydroxyl bond (O-H), which indicates the formation of $H_xWO_3$.[2,3]

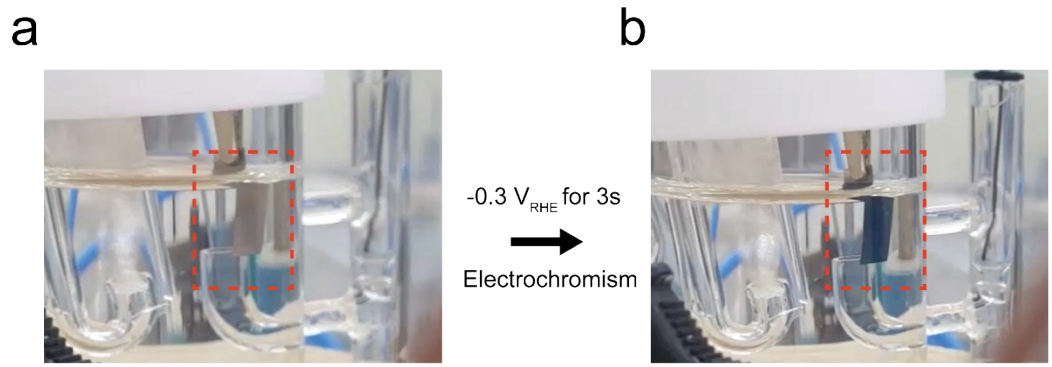


**Figure S6**. Electrochromic reaction of the $WO_3$ nanohelix sample submerged in 0.5M $H_2SO_4$ electrolyte (a) before and (b) after applying potential of −0.3 $V_{RHE}$.

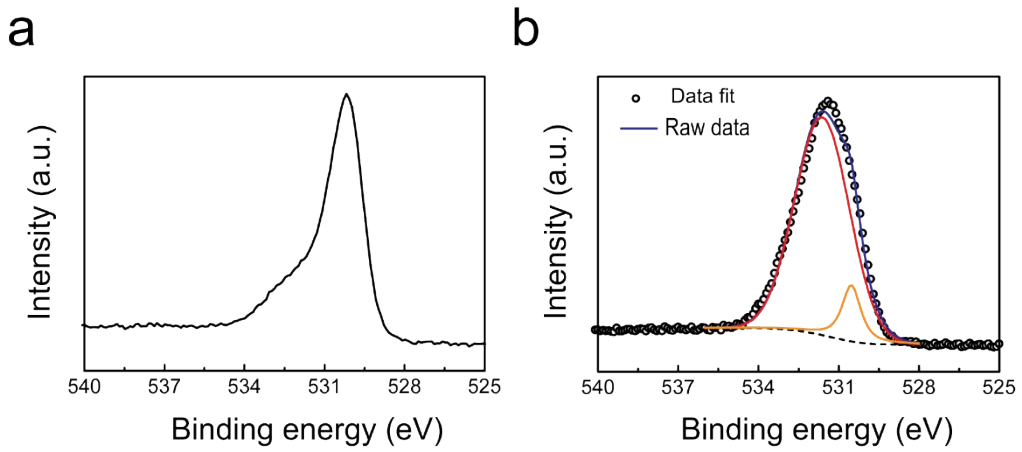


**Figure S7.** XPS spectrum of O 1s for $WS_2/WO_3$ nanotree sample (a) before and (b) after applying the −0.3 $V_{RHE}$ for 60s in 0.5 M $H_2SO_4$.

## $WS_2$ nanosheet preparation

For evaluating the catalytic activity of pure $WS_2$, $WS_2$ nanosheet was prepared through following process.
The versatile liquid phase exfoliation (LPE) method is used to prepare $WS_2$ nanosheets. Briefly the pristine $WS_2$ (Sigma Aldrich) was sonicated in N-Methyl-2-pyrrolidone (NMP), with initial concentration of 50 mg/ml was sonicated for 1 hour at 30% amplitude using a horn tip sonicator (Sonic Vibra-CV334). The solution was then centrifuged (CYROZEN 1736MGR) at 1000 rpm for 30 min to remove the contaminants (supernatant) from the starting material. The collected sediment was redispersed in fresh NMP and sonicated for 6 hours under the same condition. Which gives a polydispersed $WS_2$ solution from which the nanosheets can be isolated through cascade-centrifugation process.

The polydispersed $WS_2$ solution was first centrifuged at 500 rmp for 1 hour to remove the largest aggregates. The supernatant was then centrifuged at 1500 rpm for 1 hour and the collected supernatant was further centrifuged at 4500 rpm and collected the sediment by discarding the supernatant contains the smallest nanosheets. The sediment has been dried to remove solvents before fabricating the working electrode for electrochemical studies.

For fabricating the working electrode, $WS_2$ nanosheet powder (10mg) was mixed with the catalyst inks (water 3.98mL, IPA 1mL, Nafion 0.02mL, total 5mL), using a method reported previously.[4,5] After the solution was homogenized by sonication, the 12.5uL ink was dropped onto a tungsten foil (0.25 $cm^2$, 0.05 mm in thickness, purity: 99.95%, Nilaco, Japan,) then evaporated at room temperature to form a thin film of catalyst layer.

The fabricated WS2 working electrode was evaluated by using the three-electrode system.

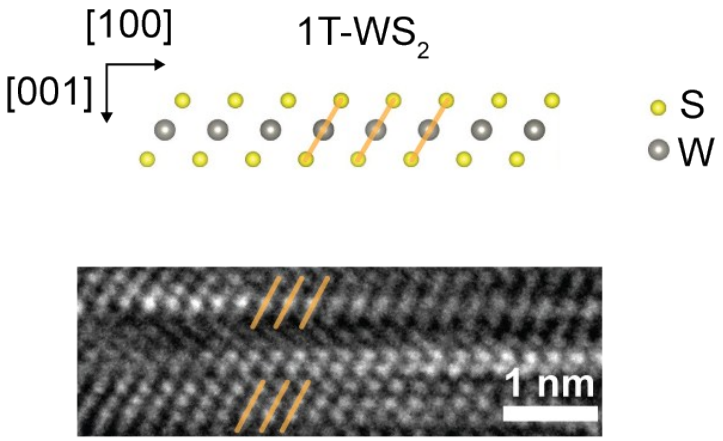


**Figure S8**. Schematic model of one S-W-S layer slab in 1T phase $WS_2$ and high-resolution TEM images of 1T phase $WS_2$. Main features of note are the linear arrangement of S-W-S atoms in the 1T phase $WS_2$, which is expressed as diagonal patterns in high-resolution TEM.

**Table S1.** Comparison of electrochemical performance for noble-metal based catalysts

| Electrodes | Onset potential [mV] | Tafel slope [mV/dec] | Overpotential (mV) at 10 mA/cm² | $R_{ct}$ [Ω] | Ref. |
|---|---|---|---|---|---|
| 20% Pt/C | N/A | 30 | 30 | N/A | 6 |
| Pt single atom-defective graphene | N/A | 25 | 23 | N/A | 6 |
| Pt-Graphdiyne | N/A | 46.6 | N/A | N/A | 7 |
| Pt-N-doped graphene nanosheets | N/A | 29 | N/A | N/A | 8 |
| $Mo_2TiC_2T_x$–Pt single atom | N/A | 30 | 30 | 12 | 9 |
| Ru-$MoO_2$ | 55 | 44 | 29 | N/A | 10 |
| Ru@N-doped C | 9.5 | 30 | 13.5 | 43.7 | 11 |
| Porous Pd NP | N/A | 30 | N/A | N/A | 12 |
| Pd nanoparticles-carbon nitride composite | 12 | 35 | 55 | N/A | 13 |
| Pd-graphene | N/A | 46 | N/A | N/A | 14 |
| Rh-$MoS_2$ | N/A | 24 | 47 | N/A | 15 |
| Ir nanowires | N/A | 30.1 | 23.1 | N/A | 16 |

**Table S2.** Comparison of electrochemical performance for TMDCs based catalysts

| Samples | Onset potential [mV] | Tafel slope [mV/dec] | Overpotential (mV) at 10 mA/cm² | $R_{ct}$ [Ω] | Ref |
|---|---|---|---|---|---|
| $WS_2$ Nanosheets with S vacancies | N/A | 83.1 | 178 | 1.81 | 17 |
| $W_2C$@$WS_2$ alloy nanoflowers | ~170 | 55.4 | N/A | ~200 | 18 |
| $WS_2$/$CoS_2$ array on Carbon cloth | N/A | 64 | 146 | N/A | 19 |
| N-enriched C foam@$WS_2$ nanoflakes | N/A | 58.7 | 153 | 3.2 | 20 |
| Te-doped $WS_2$ nanosheets | N/A | 94 | 213 | N/A | 21 |
| Nb-doped $WS_2$ nanosheets | N/A | 97 | N/A | 14.76 | 22 |
| 10% Ni-doped $WSe_2$ | N/A | 86 | 259 | N/A | 23 |
| Hierarchical $WS_2$ film | N/A | 54 | 137 | N/A | 24 |
| S-doped graphene/$WS_2$ | 140 | 53 | 250 | N/A | 25 |
| Fullerene-like $WS_2$ supported Pd nanoparticles (Pd/$WS_2$) | ~47 | 82.4 | 130 | 90 | 26 |
| 1T-$WS_2$ film | 347 | 95 | N/A | 225 | 27 |
| Edge exposed 1T phase $WS_2$/$WO_3$ Nanohelix | N/A | N/A | 168 | 8 | 28 |

| | | | | | |
|---|---|---|---|---|---|
| $WS_2/WO_3$ Nanotree | N/A | N/A | 218 | 9.8 | This work |

Reference


1 A. J. Bard and L. R. Faulkner, *Electrochemical Methods: Fundamentals and Applications, 2nd Edition*, WILEY, 2nd edn., 2000.

2 S. R. Bathe and P. S. Patil, *Solid State Ionics*, 2008, **179**, 314–323.

3 H. Wang, R. Fan, J. Miao, J. Chen, S. Mao, J. Deng and Y. Wang, *J. Mater. Chem. A*, 2018, **6**, 6780–6784.

4 J. Suntivich, H. A. Gasteiger, N. Yabuuchi and Y. Shao-Horn, *J. Electrochem. Soc.*, 2010, **157**, B1263.

5 Y. Garsany, O. A. Baturina, K. E. Swider-Lyons and S. S. Kocha, *Anal. Chem.*, 2010, **82**, 6321–6328.

6 Y. Qu, B. Chen, Z. Li, X. Duan, L. Wang, Y. Lin, T. Yuan, F. Zhou, Y. Hu, Z. Yang, C. Zhao, J. Wang, C. Zhao, Y. Hu, G. Wu, Q. Zhang, Q. Xu, B. Liu, P. Gao, R. You, W. Huang, L. Zheng, L. Gu, Y. Wu and Y. Li, *J. Am. Chem. Soc.*, 2019, **141**, 4505–4509.

7 X. P. Yin, H. J. Wang, S. F. Tang, X. L. Lu, M. Shu, R. Si and T. B. Lu, *Angew. Chemie - Int. Ed.*, 2018, **57**, 9382–9386.

8 N. Cheng, S. Stambula, D. Wang, M. N. Banis, J. Liu, A. Riese, B. Xiao, R. Li, T. K. Sham, L. M. Liu, G. A. Botton and X. Sun, *Nat. Commun.*, 2016, **7**, 1–9.

9 Jinqiang Zhang, Y. Zhao, X. Guo, C. Chen, C.-L. Dong, R.-S. Liu, C.-P. Han, Y. Li, Y. Gogotsi and G. Wang, *Nat. Catal.*, 2018, **1**, 985–992.

10 P. Jiang, Y. Yang, R. Shi, G. Xia, J. Chen, J. Su and Q. Chen, *J. Mater. Chem. A*, 2017,

**5**, 5475–5485.

11 J. Mahmood, F. Li, S. M. Jung, M. S. Okyay, I. Ahmad, S. J. Kim, N. Park, H. Y. Jeong and J. B. Baek, *Nat. Nanotechnol.*, 2017, **12**, 441–446.

12 S. Liu, X. Mu, H. Duan, C. Chen and H. Zhang, *Eur. J. Inorg. Chem.*, 2017, **2017**, 535–539.

13 T. Bhowmik, M. K. Kundu and S. Barman, *ACS Catal.*, 2016, **6**, 1929–1941.

14 S. Ghasemi, S. R. Hosseini, S. Nabipour and P. Asen, *Int. J. Hydrogen Energy*, 2015, **40**, 16184–16191.

15 Y. Cheng, S. Lu, F. Liao, L. Liu, Y. Li and M. Shao, *Adv. Funct. Mater.*, 2017, **27**, 1700359.

16 L. Fu, F. Yang, G. Cheng and W. Luo, *Nanoscale*, 2018, **10**, 1892–1897.

17 Q. Zhu, W. Chen, H. Cheng, Z. Lu and H. Pan, *ChemCatChem*, 2019, **11**, 2667–2675.

18 T. Phan, S. Young, T. Hyung, H. Won, Q. Van Le and I. T. Kim, *Appl. Surf. Sci.*, 2020, **504**, 114389.

19 J. Wu, T. Chen, C. Zhu, J. Du, L. Huang, J. Yan, D. Cai, C. Guan and C. Pan, *ACS Sustain. Chem. Eng.*, 2020, **8**, 4474–4480.

20 H. Li, A. Li, Z. Peng and X. Fu, *Appl. Surf. Sci.*, 2019, **487**, 972–980.

21 Y. Pan, F. Zheng, X. Wang, H. Qin, E. Liu, J. Sha, N. Zhao, P. Zhang and L. Ma, *J. Catal.*, 2020, **382**, 204–211.

22 M. E. Pam, J. Hu, Y. S. Ang, S. Huang, D. Kong, Y. Shi, X. Zhao, D. Geng, S. J.

Pennycook, L. K. Ang and H. Y. Yang, *ACS Appl. Mater. Interfaces*, 2019, **11**, 34862–34868.

23 S. R. Kadam, A. N. Enyashin, L. Houben, R. Bar-Ziv and M. Bar-Sadan, *J. Mater. Chem. A*, 2020, **8**, 1403–1416.

24 M. Wang, L. Zhang, M. Huang, Q. Zhang, X. Zhao, Y. He, S. Lin, J. Pan and H. Zhu, *J. Mater. Chem. A*, 2019, **7**, 22405–22411.

25 A. Kagkoura, M. Pelaez-Fernandez, R. Arenal and N. Tagmatarchis, *Nanoscale Adv.*, 2019, **1**, 1489–1496.

26 P. Xiao, J. G. Buijnsters, Y. Zhao, H. Yu, X. Xu, Y. Zhu, D. Tang, J. Zhu and Z. Zhao, *J. Catal.*, 2019, **380**, 215–223.

27 H. U. Kim, V. Kanade, M. Kim, K. S. Kim, B. S. An, H. Seok, H. Yoo, L. E. Chaney, S. Il Kim, C. W. Yang, G. Y. Yeom, D. Whang, J. H. Lee and T. Kim, *Small*, 2020, **16**, 1905000.

28 N. Lee, I. Y. Choi, K. Y. Doh, J. Kim, H. Sim, D. Lee, S. Y. Choi and J. K. Kim, *J. Mater. Chem. A*, 2019, **7**, 26378–26384.